Infrared Physics & Technology 89 (2018) 88–96

Contents lists available at ScienceDirect

Infrared Physics & Technology

journal homepage: www.elsevier.com/locate/infrared

Regular article

Infrared small target detection based on local intensity and gradient properties

Hong Zhang, Lei Zhang, Ding Yuan *, Hao Chen

Image Processing Center, Beihang University, Beijing 100191, China

HIGHLIGHTS

- Two local properties of infrared small targets from the perspective of intensity and gradient are characterized.
- The proposed model combines the intensity information and gradient information.
- Based on the two properties, an infrared small target detection algorithm is proposed.
- The proposed method yields good performance for suppressing background clutter.

ARTICLE INFO

Article history:
Received 15 July 2017
Revised 25 December 2017
Accepted 29 December 2017
Available online 30 December 2017

Keywords:
Small target detection
Gradient
Intensity
Infrared images

ABSTRACT

Infrared small target detection is a challenging task for computer vision due to the factors such as scale variations of the targets and strong clutters. Inspired by the Gaussian-like shape of the small target, we characterize two local properties of the small target from the perspective of intensity and gradient to address this problem. The two properties are that the intensity value of the target pixels is greater than the value of its locally neighboring pixels, and the gradients towards the target center often distribute regularly around the target. First, based on the two properties, the local intensity and gradient (LIG) map is calculated from the original infrared image in order to enhance the targets and suppress clutters. Next, we can obtain the targets conveniently via segmentation from the LIG map. Extensive evaluations on real data demonstrate that the proposed algorithm has satisfactory results in terms of clutter suppression and robustness.

1. Introduction

Infrared small target detection is widely applied in practical infrared imaging systems, especially in remote sensing and surveillance. Infrared small targets usually occupy a few pixels in images, and lack textural information. Since there is usually low contrast between the small targets and backgrounds in infrared images, the small targets are easily immersed in complex backgrounds [1]. Besides, the size and brightness variations of infrared small targets, which are caused by imaging distances, thermodynamic states of targets and environments, also raise the difficulty. Consequently, infrared small target detection is still a valuable research problem.

In the past decades, various methods have been proposed for detecting the small target accurately and efficiently [2–4]. The existing algorithms can be divided into three categories roughly. The first category is the target-focused method that focuses on the target characteristics and distinguishes the small targets from infrared backgrounds. High-pass filters in frequency domain have been applied to detect the targets in [5,6]. Wang et al. [5] developed two directional high-pass filtering templates by the least squares support vector machine for the detection task. Kim [6] decomposed the Laplacian of Gaussian filter into four filters and applied the minimum filter to obtain the final spatial filtering image. These methods focused on removing the low frequency clutters, but failed to filter out noise and strong clutters in the high-frequency components. A Facet-based model [7] was proposed to detect the targets based on the idea that the maximum extreme point was more likely the target, but their method neglected to preserve the shape of targets. Inspired by the human vision system (HVS), some researchers have proposed related methods. Based on local contrast, Chen et al. utilized the brightness discrepancy between the target and its neighboring area to detect the target [1]. This method could work effectively, nevertheless, it could be affected by noise of high brightness [8]. Some methods

* Corresponding author.
E-mail address: dyuan@buaa.edu.cn (D. Yuan).

https://doi.org/10.1016/j.infrared.2017.12.018
1350-4495/

reformulated the detection task as a problem of salient region detection [9]. However, strong clutters could also be salient and affect the detection results in some cases.

The second category is background-based method which concentrates on the prediction or preservation of backgrounds, and then the target is achieved by calculating the residual between the input image and the predicted background. Top-Hat transformation was widely applied in infrared small target detection [10–12]. It was firstly utilized for small targets detection in [10], but it was sensitive to noise. Afterwards, Bai et al. [13] eliminated backgrounds with a new Top-Hat transformation constructed by two different but relevant structuring elements. It obtained superior performance to the initial Top-Hat method; however, it was sensitive to the structuring elements size. Two-dimensional least mean square adaptive filters were applied to the detection in [14]. The Max-Mean and Max-Median filters were investigated for the detection problem in [15]. In their methods, the original image was filtered to estimate the background, and then the filtered image could be subtracted from the original image. Furthermore, kernel-based regression was presented to estimate the background in [16]. However, the performance of these methods which consider the background as relatively homogeneous or self-correlated is usually limited when the clutters are strong or complex.

The third category is the learning-based method. Liu et al. proposed an improved template matching method involving principal component analysis (PCA) and kernel method [17]. In [18], PCA was performed in the salient regions to detect the target. However, the training samples were generated or simulated in these methods, and the changeable appearances of small targets could degrade their performance. In [19], Gao et al. regarded the small target and the background as a sparse component and a low-rank component, respectively. In their approach, the detection was converted into recovering the two components from a data matrix. Some methods have applied sparse representation in detection recently [20,21]. However, these methods were usually time-consuming.

Different from traditional algorithms, according to the shape information of the target, we characterize two local properties of the small target from the perspective of intensity and gradient to suppress background clutters and detect infrared small targets. An infrared small target is shaped like an isotropic Gaussian intensity function because of the optics point spread function of the thermal imaging system at a long distance [9]. For intensity, the brightness value of the target is larger than the value of its locally neighboring pixels in infrared images. Additionally, for a two-dimensional Gaussian function, almost all gradients of this function point to its center. Similarly, the corresponding gradients of the infrared small target roughly point to the target center. These two properties are regarded as the local intensity property and the local gradient property respectively. The homogeneous backgrounds can be suppressed by using the local intensity property as their intensity values are nearly identical; for the backgrounds with strong edges, their gradient directions are generally consistent, hence, these gradients are different from the gradients of the target in distribution. Therefore, by combining the two properties, background clutters can be effectively suppressed. First, we calculate the local intensity and gradient (IG) map from the input infrared image. Then, we obtain the targets from the IG map via an adaptive threshold.

The remainder of this paper is organized as follows. Section 2 explicates the characteristics of local intensity and gradient (LIG) and gives the details of our method. Section 3 presents the experimental results on the real database. Finally, we draw the conclusions in Section 4.

2. Analysis and methodology

This section describes the LIG properties of infrared small targets. Meanwhile, we present the computation process of the proposed method.

2.1. Analysis of small target characteristic

Chan et al. proposed that the small target in infrared images could be modeled by a Gaussian intensity function [22]:

$$I(x,y) = \gamma e^{-\frac{1}{2}((\frac{x}{\sigma_x})^2+(\frac{y}{\sigma_y})^2)} \tag{1}$$

where γ is the peak value of the target pixels, σ_x and σ_y denote horizontal and vertical standard deviation parameters, respectively.

Infrared small targets generally occupy a few pixels in images, and lack texture and color information. However, an infrared small target is usually considered to be brighter than its surrounding background [23]. Therefore, we realize that the local intensity information is valuable for detecting the small target. The comparatively dark or homogeneous backgrounds can be suppressed by exploiting the local intensity information since their intensity values are small or nearly identical. We dub this property the local intensity property.

Additionally, considering that almost all gradient vectors of a two-dimensional Gaussian function point to its center, we realize that the gradient vectors of the target also roughly point to the target center, which is presented in Fig. 1. Moreover, the gradient directions of the backgrounds with strong edges are generally consistent. This property is viewed as the local gradient property. Accordingly, the local gradient property can be also used for detecting the small targets. As is shown in Fig. 2, some backgrounds, such as trees, have no local intensity property. Besides, the background labeled by a blue bounding box or a red bounding box is local orientated and has no local gradient property.

By virtue of the characteristics analyzed above, the intensity and gradient information is valuable for infrared small target detection.

2.2. Calculation of the LIG properties

Based on the analysis above, we give the computing process of the LIG properties as follows. First, we present the calculation of the local intensity property. Given an image patch of size $n \times n$, the average value of the local surrounding area is denoted by

$$\bar{f} = \frac{1}{1-N_m}\left(f_0 - \sum_{i=1}^{n}\sum_{j=1}^{n} f_{ij}\right), \tag{2}$$

where N_m is the pixel number in an image patch. f_{ij} denotes the value of each pixel in the patch, and f_0 represents the value of its center pixel. Further, we can achieve the local intensity value of an image patch by

$$I = \max(0, f_0 - \bar{f}). \tag{3}$$

For an infrared small target, its gray value is normally larger than that of its surrounding pixels [23], thus $I > 0$. Whereas, the clutter whose value of the center pixel is smaller than the local mean can be suppressed.

After I is achieved, we divide the image patch into four parts along the radial direction, and set the center of the patch as the origin to establish a polar coordinate system. Each part can be expressed by

$$\Psi_i = \left\{(\gamma,\theta_i)|\frac{\pi(i-1)}{2} < \theta_i \leqslant \frac{\pi i}{2}\right\}, \tag{4}$$

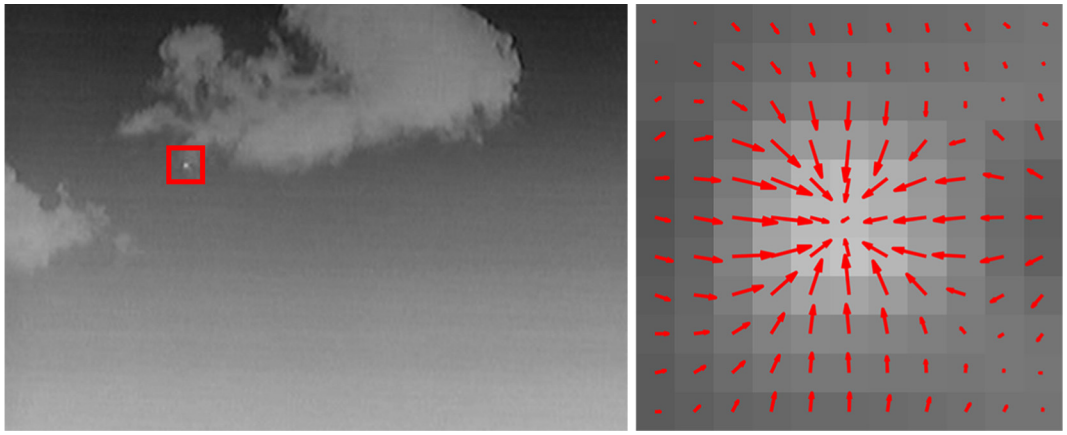

Fig. 1. An infrared small target and its gradient vectors.

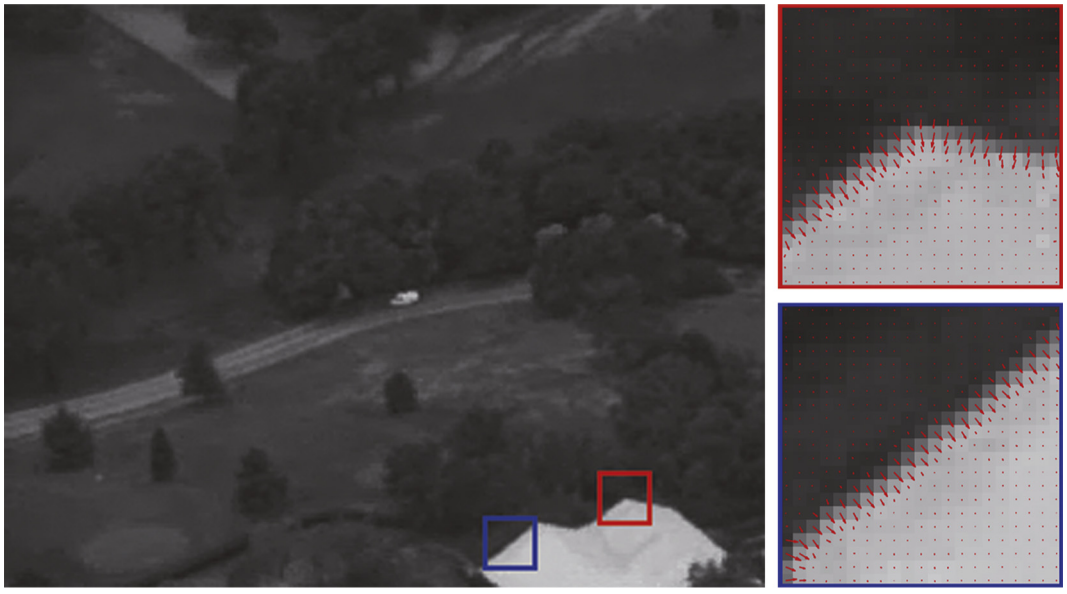

Fig. 2. A small target along with ground clutters and the enlarged clutters along with the gradient vectors.

where Ψ_i represents the i_{th} $(i = 1, 2, 3, 4)$ part in the patch, and (γ, θ_i) is a point in the polar coordinate system of the patch. Since that the gradients of the small target do not point to its center so strictly, thus a relatively loose constraint is used to formulate the gradients towards the center

$$\Phi_{\Psi_i} = \left\{ g_{\Psi_i}(m, \alpha, \gamma, \theta_i) \middle| \frac{\pi(i-1)}{2} + \pi < \alpha \leqslant \frac{\pi i}{2} + \pi, (\gamma, \theta_i) \in \Psi_i \right\}, \tag{5}$$

where Φ_{Ψ_i} represents the set of the gradients that satisfy the constraints in the region Ψ_i, and $g_{\Psi_i}(m, \alpha, \gamma, \theta_i)$ is the gradient element in the set Φ_{Ψ_i}. m and α represent the magnitude and direction of g_{Ψ_i}, respectively. Fig. 3 presents an example of g_{Ψ_i}. g_1 and g_2 are two gradients in Ψ_1. According to constraint (5), the gradient in Ψ_1 will be selected only if its direction meets the constraint $\pi < \alpha \leqslant 1.5\pi$. So $g_1 \in \Phi_{\Psi_1}$, while $g_2 \notin \Phi_{\Psi_1}$.

Then, in each region, calculate the mean square of g_{Ψ_i} amplitudes. It is defined as follows:

$$G_i = \frac{1}{N_j} \sum_{j=1}^{N_j} \|g_{\Psi_i}^j\|^2, \tag{6}$$

where N_j $(j = 1, 2, \ldots, N_j)$ is the number of g_{Ψ_i} in the set Φ_{Ψ_i}.

After all G_i are acquired, their maximum value and minimum value can be gained by

$$G_{\max} = \max_{1 \leqslant i \leqslant 4} G_i, \tag{7}$$

$$G_{\min} = \min_{1 \leqslant i \leqslant 4} G_i, \tag{8}$$

where $G_{\max}$ and $G_{\min}$ are the maximum and minimum of G_i respectively. Furthermore, all of G_i in an image patch can be accumulated as

$$G = \begin{cases} \sum_{i=1}^{4} G_i, & \text{if} \quad \frac{G_{\min}}{G_{\max}} > k, \\ 0, & \text{otherwise}, \end{cases} \tag{9}$$

where G represents the local gradient value of an image patch, and k is obtained from experiments. Since that the small targets in infrared images have isotropic Gaussian-like shape, their gradient directions are evenly distributed in all directions. Whereas, background clutters are generally local orientated [9]. Thus, the local orientated clutter can be suppressed by utilizing the ratio of $G_{\min}$ and $G_{\max}$. The process of computing I and G is shown in the Algorithm 1, where the

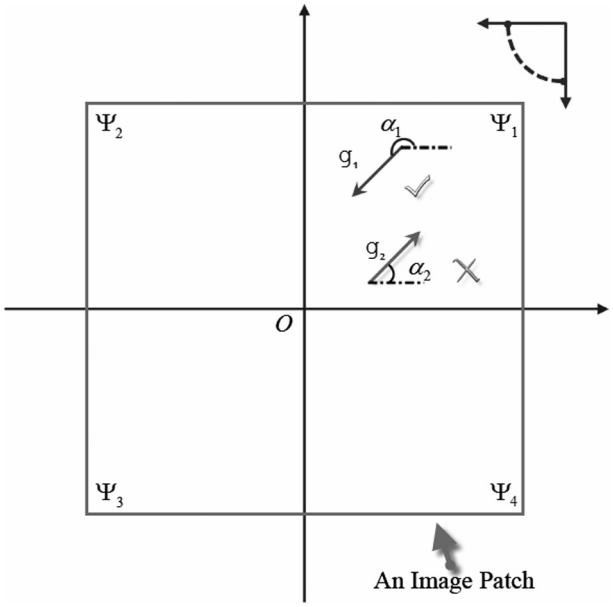

Fig. 3. Illustration of g_{Ψ_i}. An image patch is divided into four regions denoted by Ψ_1 to Ψ_4. g_1 and g_2 are two gradients in Ψ_1. g_1 points to the center roughly, while g_2 does not. According to constraint (5), $g_1 \in \Phi_{\Psi_1}$ and $g_2 \notin \Phi_{\Psi_1}$.

patch size should be larger than or approximate to the target size. The number of pixels for a small target is generally less than 80 [1]. Therefore, we fix the sliding window size with 11×11 which is larger than the target size in most cases. The process of computing I and G can be calculated in parallel, and the computation of G_i in each region is independent of each other. Through these steps above, I and G value of an image patch can be obtained.

Algorithm 1. Calculation process of I and G.

Input: Infrared image patch of size $n \times n$.

1: Get f_0 and compute $\bar{f}$

$$\bar{f} = \frac{1}{1 - N_m}\left(f_0 - \sum_{i=1}^{n}\sum_{j=1}^{n} f_{ij}\right),$$

2: Compute the local intensity value

$$I = \max(0, f_0 - \bar{f}).$$

3: **for** $i = 1, 2, 3, 4$ **do**

$$G_i = \frac{1}{N_j}\sum_{j=1}^{N_j} \|g_{\Psi_i}^j\|^2,$$

4: **end for**

5: Compute the maximum and minimum of G_i

$G_{\max} = \max_{1 \leqslant i \leqslant 4} G_i, \quad G_{\min} = \min_{1 \leqslant i \leqslant 4} G_i.$

6:

$$G = \begin{cases} \sum_{i=1}^{4} G_i, & \text{if } \frac{G_{\min}}{G_{\max}} > k, \\ 0, & \text{otherwise}, \end{cases}$$

Output: I and G.

2.3. Target detection based on LIG algorithm

Fig. 4 illustrates the overview of our method. First, image patches are achieved from the input infrared image with a sliding window of size $n \times n$. The stride is 1 pixel. Then, I map and G map can be achieved by calculating I value and G value for each patch according to Algorithm 1. Besides, the detection process is shown in Algorithm 2, where $IG_{i,j}, I_{i,j}$, and $G_{i,j}$ are the pixel value in IG map, I map, and G map respectively; W and H denote the width and height of the maps; $\overline{IG}_{i,j}$ denotes the mean value of non-zero pixels in the IG map. T represents the adaptive threshold.

Algorithm 2. Process of detection by LIG method.

Input: Infrared image frame.

1: Obtain image patches by a sliding window.
2: Compute each I and G according to Algorithm 1.
3: Normalize I map and G map.
4: **for** i = 1:W **do**
5: **for** j = 1:H **do**

$$IG_{i,j} = I_{i,j} \times G_{i,j}.$$

6: **end for**
7; **end for**
8: Calculate the threshold by

$$T = \overline{IG}_{i,j}.$$

9: Obtain the segment result by the threshold T.
Output: Target position.

Before the multiplication, I map and G map are normalized to a range of 0–1 respectively. However, this process can be omitted, because of little effect on the results. It is worth to mention that we only discuss the bright target. To detect the dark one, the only need is to reverse the conditions in (3) and (5). For the pixel in the IG map, the larger value it has, the more likely it is a target. Finally, the targets can be obtained from the IG map by using the adaptive threshold.

3. Experimental evaluations

First, we discuss the effects of parameters on our method. Then, we compare our method with some other methods to evaluate the performance.

3.1. Effects of parameters

In this section, we discuss the effects of the window size and the ratio parameter k, respectively. In the experiments, we use 50 infrared images with various backgrounds, including cloud, sea, and ground. Fig. 5 presents the samples. The largest size of the targets in these images is about 10×8 pixels.

We draw the receiver operation characteristic (ROC) curves [24] to visualize the capability of different parameters. The ROC curve depicts the relative relationship between true positives and false positives. True positive rate P_d (detection probability) and false positive rate P_f (false alarm rate) are calculated as:

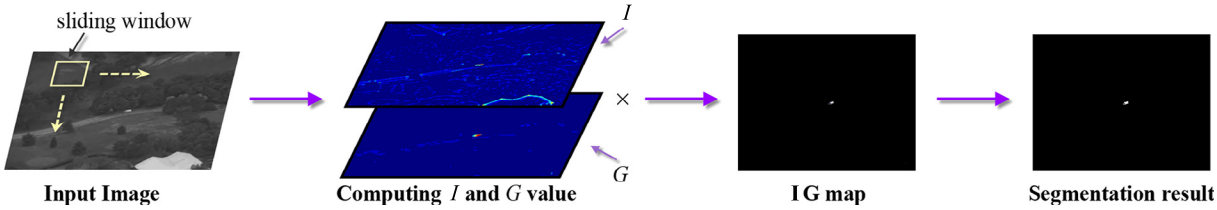

Fig. 4. The overview of the proposed method.

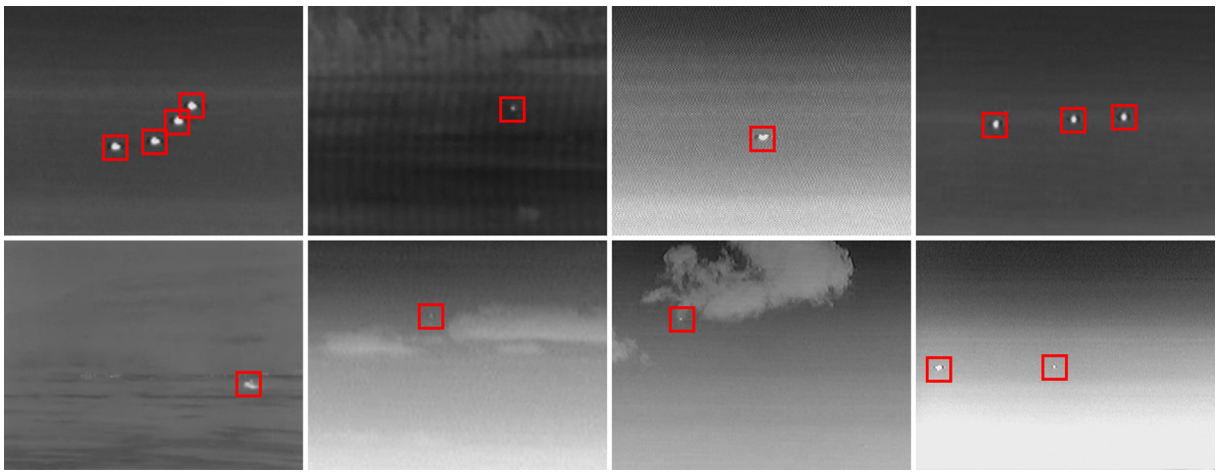

Fig. 5. The samples of the test images.

$$P_d = \frac{\text{number of detected detections}}{\text{number of real targets pixels}}, \tag{10}$$

$$P_f = \frac{\text{number of false alarms}}{\text{number of total pixels}}. \tag{11}$$

Accordingly, we hope that P_d has a large value while P_f has a small one. Generally, the upper-left curve (P_d is higher, P_f is lower, or both) in a graph is better. More detailed information on ROC graph can be found in [25].

In the first experiment, we fix the ratio parameter k as 0.2 and test the proposed method with different window sizes. Fig. 6 illustrates the corresponding ROC curves [24]. As the window size increases, the results can be better. When the window size exceeds the target size (about 10×8), the performance does not change too much, which is attributed to the utilization of the mean square of the gradients satisfied (5). When the target appears in the current patch and the patch size exceeds the target size, even if the patch size is increased, the statistic of the gradients will change little without new gradient meeting the constraint. As mentioned above, the target size is not constant, and it is usually affected by the target type, imaging distance, and so on. The multi-scale operation was applied to solve the problem in [1,19]. Although it can solve

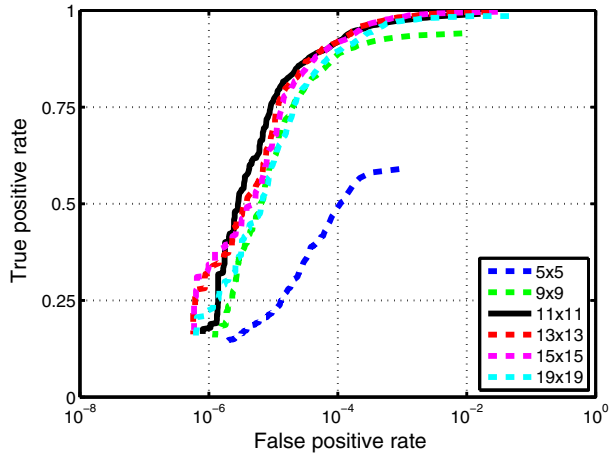

Fig. 6. The ROC curves of different window sizes.

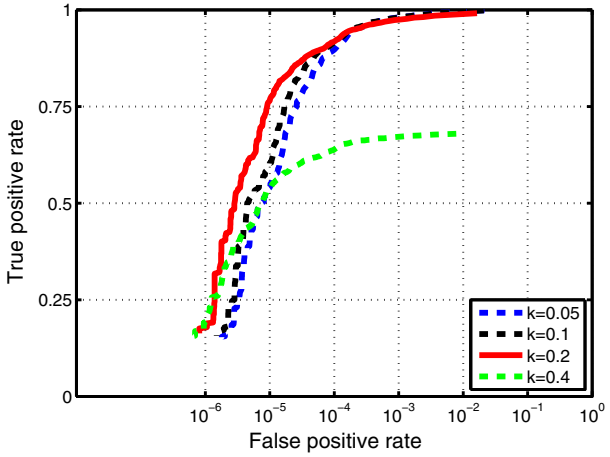

Fig. 7. The ROC curves of different parameter k.

Table 1
Detailed information of four sequences.

Seq.	Background	Image size	Target size
1	Sky-cloud	352 × 288	about 2 × 3
2	Sky-cloud,noise	352 × 288	about 3 × 3
3	Cloud clutter	320 × 240	about 10 × 4
4	Ground	320 × 240	about 10 × 5

the problem of varied scales of small targets, it brings much extra computation. In the proposed algorithm, we only use the sliding window of one scale, and its size only needs to be larger than or closer to the target size.

Then, we fix the window size of 11 × 11, and test our method with different k, whose ROC curves are presented in Fig. 7. As k is increased to 0.2, the performance gets better, which indicates that more clutters are suppressed when utilizing a bigger k. How-

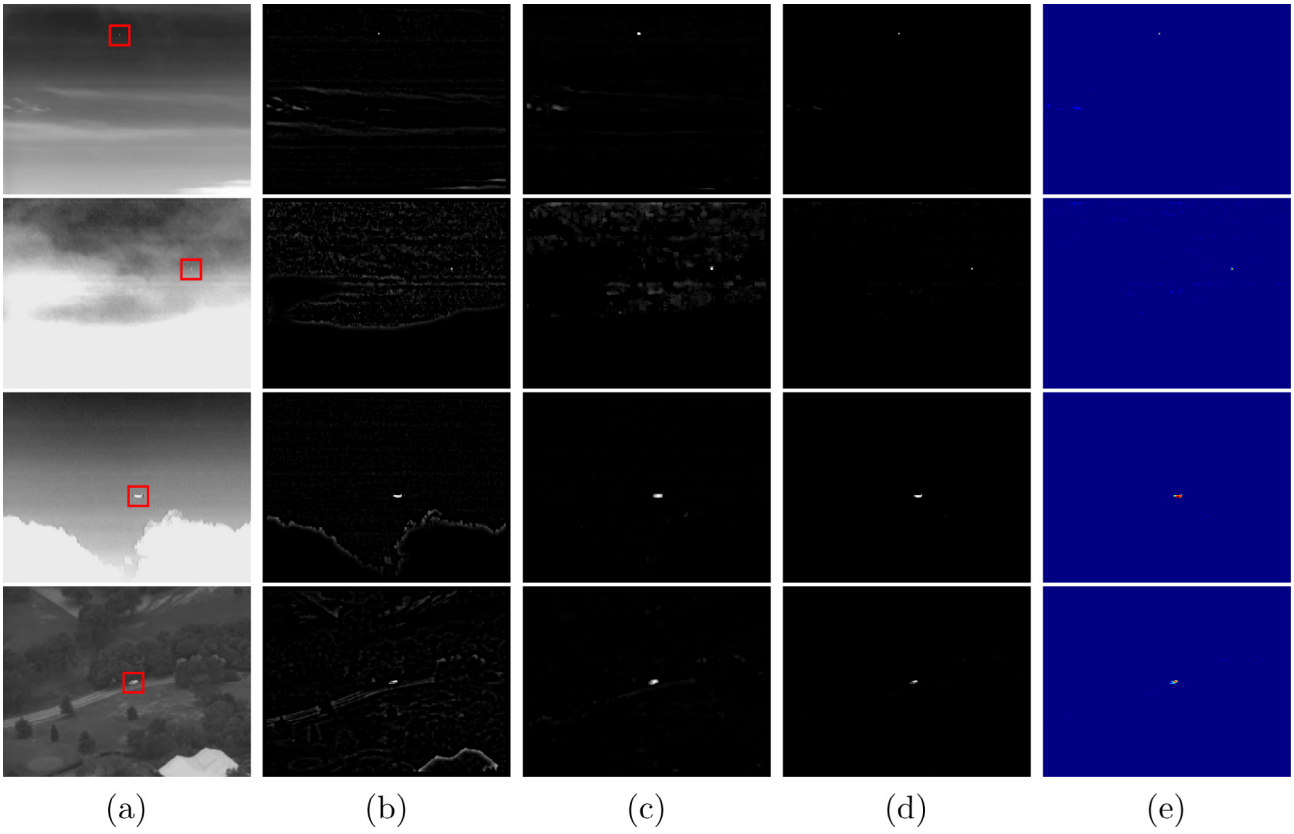

Fig. 8. The representative results of the four sequences of the proposed algorithm. (a) The original images. (b) Maps of the local intensity property. (c) Maps of the local gradient property. (d) IG maps of the proposed method. (e) IG maps with pseudo-color. (For interpretation of the references to colour in this figure legend, the reader is referred to the web version of this article.)

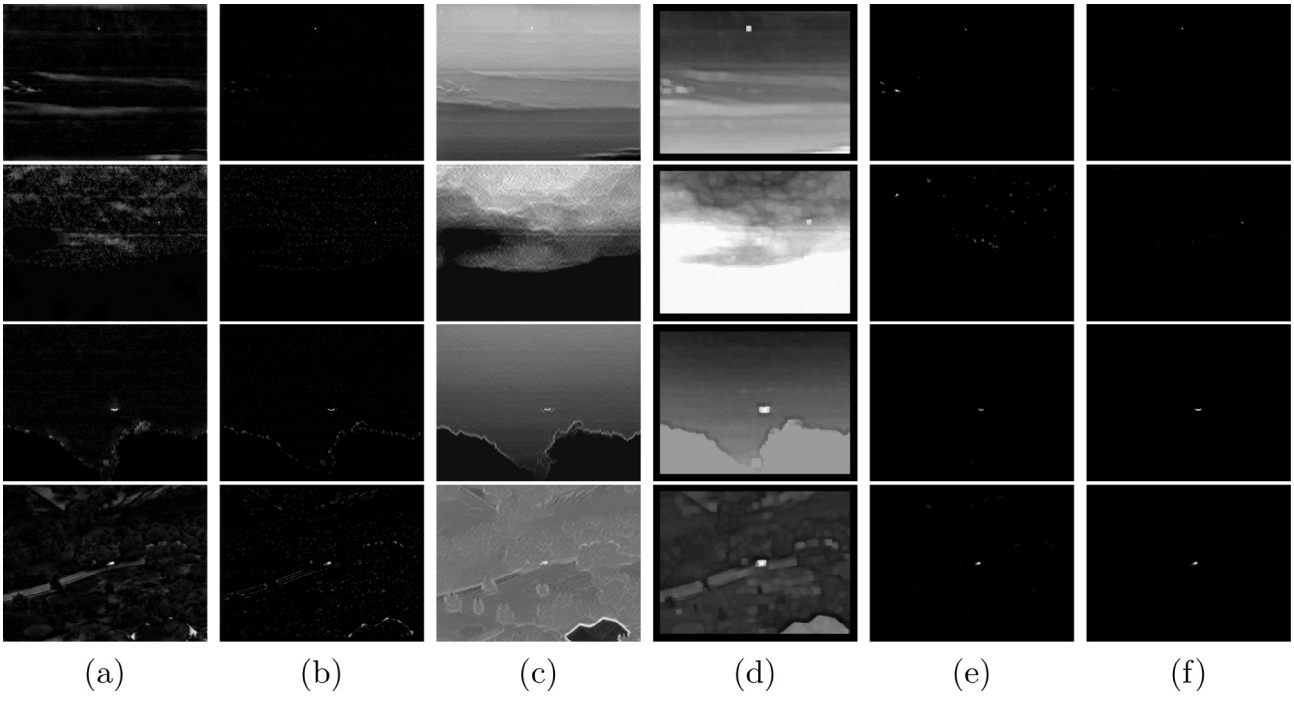

Fig. 9. The resultant images with different methods. (a) Filtered results of Top-Hat. (b) Filtered results of Max-Mean. (c) Filtered results of MILL. (d) Maps of LCM. (e) Maps of MPCM. (f) IG maps of the proposed method. The same raw infrared images as Fig. 8(a) are used.

ever, the performance degrades a lot when k value is set to 0.4, because too large k can also suppress parts of the targets that are not shaped like a Gaussian function strictly. Finally, we set k as 0.2 in our method.

3.2. Contrast experiment

To assess the capability of our method, four sets of infrared images are used in the experiments. The four infrared sequences selected are with various backgrounds, and the target size is not constant in the sequence. Each sequence contains 100 images. For simplicity, the four sequences are denoted by Seq. 1 to Seq. 4 respectively. Table 1 shows detailed information of these sequences. Seq. 1 and Seq. 3 contain sky cloudy background. Seq. 2 contains cloud clutters with noise, whereas backgrounds of Seq. 4 comprise trees, roads, and buildings.

We compare the proposed algorithm with other five methods to validate the detection performance. Among copious methods, we choose the traditional Top-Hat filter method[10], Max-Mean[15], the min-local-log (MILL) [6], the local contrast method (LCM)[1] and the multi-scale patch-based contrast measure (MPCM)[26] for comparison. All the above algorithms are calculated in the spatial domain and have a low computational cost. Our experiments are conducted on a computer with an Intel i5-4460 CPU (3.2 GHz) PC and 8 GB memory. Our method implemented in MATLAB runs at about 1.4s/frame in the experiments.

Fig. 8 illustrates the representative results of the four sequences of our algorithm. Fig. 8(a) presents representative images from infrared sequences. The sliding window size of the proposed method is set to 11×11, and the parameter k is set to 0.2. We use the same parameter values for all the sequences. It can be seen that the local intensity property is likely to suppress the cloud background better, and the local gradient property is efficient in eliminating the strong edges. It is unable to completely eliminate clutters if only a single property of the LIG method is used. Although some clutters may still own a certain property of the LIG characteristics, the small targets have the LIG characteristics simultaneously in infrared images. By combining I and the corresponding G, the background clutters are suppressed greatly in IG maps.

Fig. 9 illustrates the corresponding results of these methods. The test images are the same as the test images in Fig. 8. It can be seen that Top-Hat can enhance the targets successfully, but it fails in suppressing the clutters. Max-Mean seems to be more effective for the spot-like targets, but for Seq. 3 and Seq. 4, it does not filter out the edges of the clutters successfully. For MILL, it does

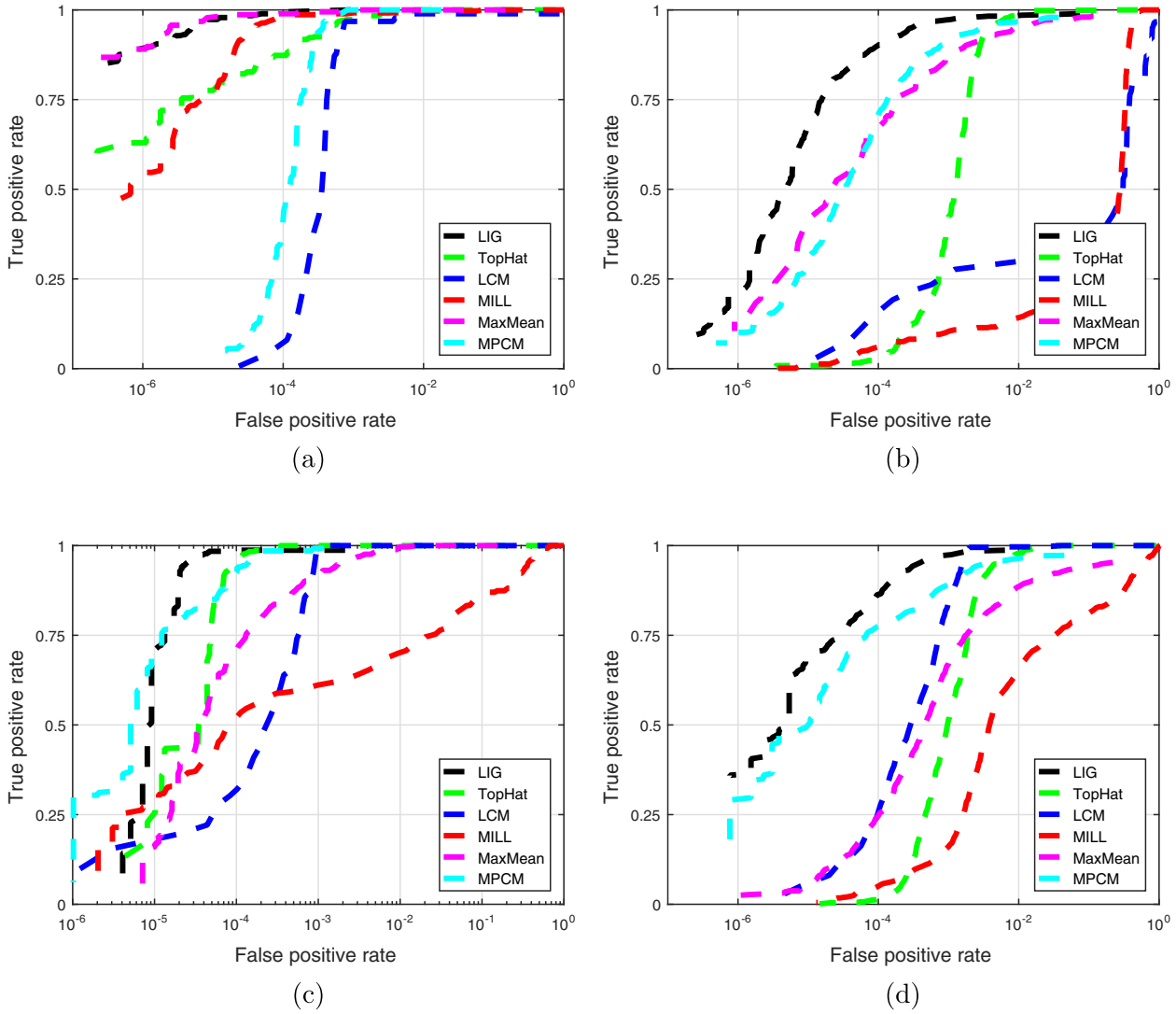

Fig. 10. ROC curves obtained by each method for Seq. 1 to 4. (a)–(d) are the ROC graphs for Seq. 1 to 4, respectively.

Table 2
The average results of different detection methods for each sequence. Bold fonts indicate the best performance.

Seq.	Indicators	Top-Hat	Max-Mean	MILL	LCM	MPCM	Proposed
1	$\overline{\text{SCRG}}$	102.94	636.25	18.80	28.52	219.88	**11491.72**
	$\overline{\text{BSF}}$	5.97	30.57	1.44	1.41	17.95	**835.61**
2	$\overline{\text{SCRG}}$	50.31	280.87	7.58	16.86	144.76	**7435.16**
	$\overline{\text{BSF}}$	5.99	17.81	1.33	1.27	38.79	**423.56**
3	$\overline{\text{SCRG}}$	56.85	289.65	8.52	17.00	182.77	**7518.48**
	$\overline{\text{BSF}}$	7.04	19.74	1.55	1.38	50.51	**395.11**
4	$\overline{\text{SCRG}}$	51.14	281.15	8.33	16.76	139.60	**7429.01**
	$\overline{\text{BSF}}$	4.61	15.82	1.61	1.21	27.66	**367.59**

not cope with the edges very well. LCM can enhance the target successfully, but for Seq. 1 and Seq. 2, the backgrounds with high brightness are not suppressed. MPCM achieves satisfactory results for Seq. 3 and Seq. 4, but it fails to filter out the messy clutters. For the proposed algorithm, most of the backgrounds of the four sequences are suppressed in IG maps, which indicates that the threshold requirement of our method is less stringent. Besides, our method maintains the shape information well for small targets in different sizes.

Fig. 10 demonstrates the ROC results for the five methods on the four sequences. We can see that our method obtains superior results compared to other methods. For Seq. 1 and Seq. 2, Max-Mean performs considerably well, which also indicates that it has better performance for the spot-like targets than large ones. For Seq.3, MPCM performs a little better than our method at the beginning, but our method can reach 1 faster than MPCM. For Seq. 4, MPCM also achieves good performance. By comparison, our method achieves better results in all the sequences, which demonstrates that our method is stable for different target sizes and different clutters.

In addition, we also choose two common evaluation indicators for comparison, which are signal-to-clutter ratio gain (SCRG) and background suppression factor (BSF). The indicators are defined as follows:

$$\text{SCRG} = \frac{(S/C)_{out}}{(S/C)_{in}}, \qquad \text{BSF} = \frac{C_{in}}{C_{out}} \tag{12}$$

where S represents the signal amplitude, and C is clutter standard deviation. The details of the two metrics can be found in [27]. To a certain extent, SCRG can measure clutter suppression and target preservation, and BSF is metric which reflects the performance for clutter removal without the target information [27]. Generally, the higher the SCRG is, the stronger ability of clutter suppression and target enhancement the method has.

Table 2 presents the average results of different methods for each sequence. $\overline{\text{SCRG}}$ and $\overline{\text{BSF}}$ represent the average results. It can be seen that Top-Hat, Max-Mean, and MPCM achieve a better performance than the other baseline methods, because they have the steps of backgrounds prediction or preservation, and the predicted backgrounds are subtracted from the original image. Thus, they can achieve large $\overline{\text{SCRG}}$ and $\overline{\text{BSF}}$. However, MILL and LCM do not specialize in the background suppression, thus their performance is not superior to others. The proposed approach achieves the best performance on the two metrics. $\overline{\text{SCRG}}$ and $\overline{\text{BSF}}$ of our method are large extremely, because the majority of backgrounds are directly set as 0 in (3) and (9), the clutters are suppressed well, and small C_{out} is achieved.

4. Conclusion

Infrared small target detection still suffers from scale variations of the targets and strong clutters. Motivated by the fact that an infrared small target is approximately shaped like a two-dimensional Gaussian function, we characterize the local intensity and gradient properties to detect infrared small targets. The experiments on real data indicate that our method has not only the capability of suppressing the clutters, but also good performance and robustness for various target sizes. The combination of the two properties can detect the target more effectively. As further works, we will try to combine our method with the motion information of the target to strive for further improvement in this field.

Funding

This work was supported by the National Natural Science Foundation of China [Grant No. 61571026] and the National Key Research and Development Program of China [Grant No. 2016YFE0108100].

Conflict of interest

None.

References

[1] C.P. Chen, H. Li, Y. Wei, T. Xia, Y.Y. Tang, A local contrast method for small infrared target detection, IEEE Trans. Geosci. Remote Sens. 52 (1) (2014) 574–581.
[2] H. Qin, J. Han, X. Yan, Q. Zeng, H. Zhou, J. Li, Z. Chen, Infrared small moving target detection using sparse representation-based image decomposition, Infrared Phys. Technol. 76 (2016) 148–156.
[3] J. Han, Y. Ma, J. Huang, X. Mei, J. Ma, An infrared small target detecting algorithm based on human visual system, IEEE Geosci. Rem. Sens. Lett. 13 (3) (2016) 452–456.
[4] K. Shang, X. Sun, J. Tian, Y. Li, J. Ma, Infrared small target detection via line-based reconstruction and entropy-induced suppression, Infrared Phys. Technol. 76 (2016) 75–81.
[5] P. Wang, J. Tian, C.Q. Gao, Infrared small target detection using directional highpass filters based on LS-SVM, Electron. Lett. 45 (3) (2009) 156–158.
[6] S. Kim, Min-local-LoG filter for detecting small targets in cluttered background, Electron. Lett. 47 (2) (2011) 105–106.
[7] G.-D. Wang, C.-Y. Chen, X.-B. Shen, Facet-based infrared small target detection method, Electron. Lett. 41 (22) (2005) 1244–1246.
[8] J. Han, Y. Ma, B. Zhou, F. Fan, K. Liang, Y. Fang, A robust infrared small target detection algorithm based on human visual system, IEEE Geosci. Remote Sens. Lett. 11 (12) (2014) 2168–2172.
[9] S. Qi, J. Ma, C. Tao, C. Yang, J. Tian, A robust directional saliency-based method for infrared small-target detection under various complex backgrounds, IEEE Geosci. Remote Sens. Lett. 10 (3) (2013) 495–499.
[10] V.T. Tom, T. Peli, M. Leung, J.E. Bondaryk, Morphology-based algorithm for point target detection in infrared backgrounds, in: Proc. SPIE, Vol. 1954, 1993, pp. 25–32.
[11] U. Braga-Neto, M. Choudhary, J. Goutsias, Automatic target detection and tracking in forward-looking infrared image sequences using morphological connected operators, J. Electron. Imag. 13 (4) (2004) 802–813.
[12] M. Zeng, J. Li, Z. Peng, The design of top-hat morphological filter and application to infrared target detection, Infrared Phys. Technol. 48 (1) (2006) 67–76.
[13] X. Bai, F. Zhou, Analysis of new top-hat transformation and the application for infrared dim small target detection, Pattern Recognit. 43 (6) (2010) 2145–2156.

[14] T. Soni, J.R. Zeidler, W.H. Ku, Performance evaluation of 2-D adaptive prediction filters for detection of small objects in image data, IEEE Trans. Image Process. 2 (3) (1993) 327–340.
[15] S.D. Deshpande, H.E. Meng, R. Venkateswarlu, P. Chan, Max-mean and max-median filters for detection of small targets, in: Proc. SPIE, Vol. 3809, 1999, pp. 74–83.
[16] Y. Gu, C. Wang, B. Liu, Y. Zhang, A kernel-based nonparametric regression method for clutter removal in infrared small-target detection applications, IEEE Geosci. Remote Sens. Lett. 7 (3) (2010) 469–473.
[17] R. Liu, Y. Lu, C. Gong, Y. Liu, Infrared point target detection with improved template matching, Infrared Phys. Technol. 55 (4) (2012) 380–387.
[18] T. Hu, J.-J. Zhao, Y. Cao, F.-L. Wang, J. Yang, Infrared small target detection based on saliency and principle component analysis, J. Infrared Millim. Waves 29 (4) (2010) 303–306.
[19] C. Gao, D. Meng, Y. Yang, Y. Wang, X. Zhou, A. Hauptmann, Infrared patch-image model for small target detection in a single image, IEEE Trans. Image Process. 22 (12) (2013) 4996–5009.
[20] J. Zhao, J. Chen, Y. Chen, H. Feng, Z. Xu, Q. Li, Sparse-representation-based automatic target detection in infrared imagery, Infrared Phys. Technol. 56 (2013) 85–92.
[21] Z.-Z. Li, J. Chen, Q. Hou, H.-X. Fu, Z. Dai, G. Jin, R.-Z. Li, C.-J. Liu, Sparse representation for infrared dim target detection via a discriminative over-complete dictionary learned online, Sensors 14 (6) (2014) 9451–9470.
[22] D.S. Chan, D.A. Langan, D.A. Staver, Spatial-processing techniques for the detection of small targets in IR clutter, in: Proc. SPIE, Vol. 1305, 1990, pp. 53–62.
[23] S. Qi, D. Ming, J. Ma, X. Sun, J. Tian, Robust method for infrared small-target detection based on boolean map visual theory, Appl. Opt. 53 (18) (2014) 3929–3940.
[24] S. Qi, J. Ma, H. Li, S. Zhang, J. Tian, Infrared small target enhancement via phase spectrum of quaternion fourier transform, Infrared Phys. Technol. 62 (2014) 50–58.
[25] T. Fawcett, An introduction to ROC analysis, Pattern Recognit. Lett. 27 (8) (2006) 861–874.
[26] Y. Wei, X. You, H. Li, Multiscale patch-based contrast measure for small infrared target detection, Pattern Recognit. 58 (2016) 216–226.
[27] C.I. Hilliard, Selection of a clutter rejection algorithm for real-time target detection from an airborne platform, in: Proc. SPIE, Vol. 4048, 2000, pp. 74–84.